

Propagation Characteristics of Groove Gap Waveguide Below and Above Cutoff

Antonio Berenguer¹, Vincent Fusco², Dmitry Zelenchuk², Daniel Sanchez-Escuderos¹, Mariano Baquero-Escudero¹, Vicente E. Boria Esbert¹, Alejandro Valero-Nogueira, Miguel Ferrando-Bataller, Miguel Ferrando-Rocher, Tomás Bernabeu-Jiménez, Felipe Vico.

¹Instituto de Telecomunicaciones y Aplicaciones Multimedia
Universitat Politècnica de València Valencia (46022) Spain anbever@iteam.upv.es

²The Institute of Electronics, Communications and Information Technology
Queen's University of Belfast
Belfast (BT3 9DT) United Kingdom

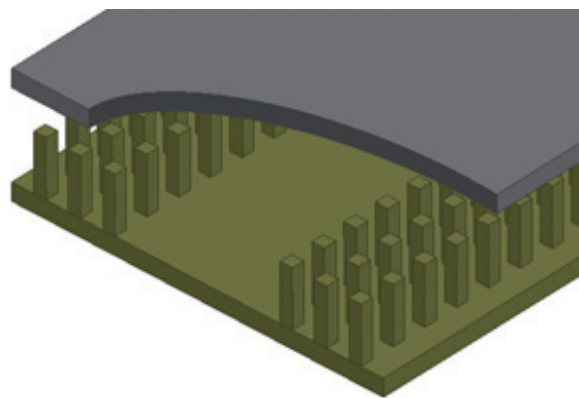
Abstract

Recently, gap waveguides have been shown as a potential alternative to conventional waveguides in the millimeter-wave band. Until now, Groove Gap Waveguide (GGW) has been studied through direct correspondence with rectangular waveguide with the same physical dimensions. However there have been observed differences in the above cutoff propagation characteristics between these two waveguide types. Furthermore, the behavior of GGW below cutoff remains unknown. This work presents a discussion of both below and above cutoff propagation characteristics of GGW, and introduces a simple model that explains the observed GGW behavior and establishes well its propagation characteristics. Two TRL calibration kits have been manufactured, and the measurements have good agreement with the proposed analysis model results.

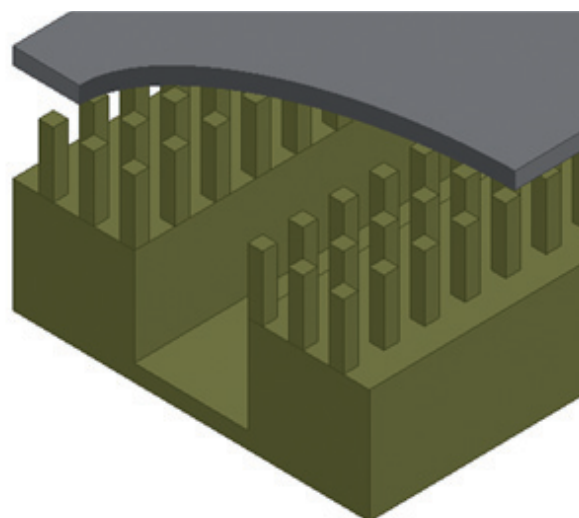
Index Terms: groove gap waveguide, transmission lines, characteristic impedance, evanescent propagation.

1. Introduction

The millimeter-wave band [1]-[4] continues to attract the interest of the research community, as new applications consistently demand the development of suitable components operating in this high frequency range. At millimeter-wave bands, dielectric materials can have high losses [5]-[6] and coupling to substrate modes [7]-[8] can be problematical. Recently, as an attempt to solve these problems, Gap Waveguides (GW) were proposed [9]-[10]. GW are based on the use of a periodic structure, usually realized by square metal pins, shown in Fig. 1. The pin lattice introduces a high impedance condition at the plane above the pins. Thus, by placing a metal plate



(a) GGW-VP.



(b) GGW-HP.

■ **Figure 1.** Groove Gap waveguides.

GGWs have shown their potential advantage versus conventional waveguides through prototypes, including couplers filters and antennas.

at a distance $h_a < \lambda/4$ from the top of the pins, no wave can propagate in this region over a certain frequency range, defined by the periodic lattice parameters. Groove Gap Waveguide (GGW) can take two versions, vertical polarization (VP), Fig. 1(a), and horizontal polarization (HP), Fig. 1(b). Both versions behave in a similar way as a rectangular waveguide, propagating a quasi-TE mode [9]-[11].

GGWs have shown their potential advantage versus conventional waveguides through prototypes, including couplers, filters and antennas [12]-[15]. However, at this moment, although the behavior of the periodic lattice is characterized [16], it seems that more efforts are necessary in the development of simple models that explain better GGW propagation characteristics especially close to, and below, cutoff.

The difficulty in characterizing gap waveguides arises from the presence of the periodic pin structure, which leads to a waveguide which is not homogeneous in the transversal direction, is periodic in the propagation direction, and has many design parameters. Homogenization of the structure based on metamaterial analogies has led to analytical models [17]-[19]. However, unlike metamaterials, the periodic structure in GGW is comparable with the operating wavelength, thus calling into question their general applicability.

In fact, the propagation characteristics of GGW have not been analyzed in great detail. Usually, it is assumed that GGW behaves like a rectangular waveguide with the same propagation channel dimensions [20]. However, in this paper, important differences between GGW and rectangular waveguide will be shown to exist. To the authors' knowledge, the GGW behavior near to, or below, the cutoff frequency has not been reported up to now. There are many practical applications using below-cutoff waveguides, since evanescent-mode components can be very compact, and are very appropriate to exhibit spurious free response [21]-[24].

Therefore, the main aim of this paper is to address the aforementioned questions. In particular, a simple model that shows very good agreement with full-wave results, and provides a simple explanation of how GGW operates, is presented. This model is also useful as a tool for extracting the influence of the different waveguide parameters in the dispersion diagram through fast parametric analysis, thus avoiding the need for very time consuming full-wave EM simulations. The remainder of this paper will focus on GGW-VP¹, which is the option, to date, chosen to implement high quality resonators [25] and low insertion loss filters [13], [14].

The paper is organized as follows. In section 2 the Groove Gap Waveguide is reminded, and its propagation

characteristics are studied both below and above cutoff. The observed differences between GGW and classical rectangular waveguide are discussed. In section 3, a simple propagation model is proposed and the results obtained are shown. In Section 4, the proposed model is successfully validated by means of experimental measurements of two GGW prototypes. Finally, conclusions and overall remarks are given.

2. The Groove Gap Waveguide

The Groove Gap Waveguide was firstly proposed in [9]. Fig. 2 shows the transverse view of this type of waveguide, its main geometrical parameters and the field distribution of its fundamental propagating mode. The periodic structure inhibits propagation in lateral directions, and imposes a propagation mode similar to the TE₁₀ mode of standard rectangular waveguide.

Although the lateral periodic structures should be of infinite extension ideally, in practice they can be significantly truncated without significant loss of performance. Three rows of pins have been shown to be enough in order to achieve the desired effect of forbidden propagation in the lateral regions [13], [25].

A. Operation above cutoff

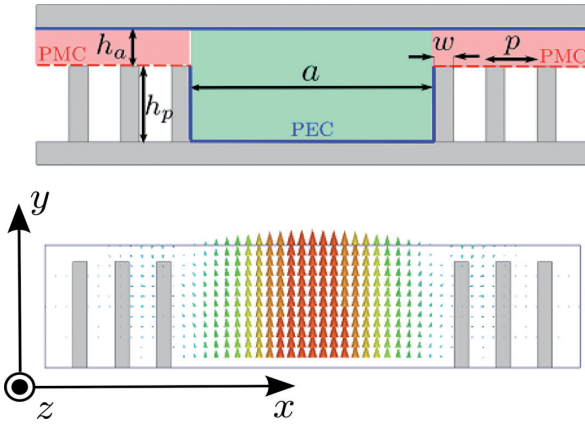
To analyse the dispersion diagram of the structure, the dimensions used in [13] are taken as a reference. These dimensions are $h_p = 2.4$ mm, $w = 0.3$ mm, $p = 0.9$ mm, $h_a = 0.375$ mm and $a = 4.7$ mm. The full-wave simulations are carried out using CST[®] [26]. Fig. 3 shows the propagation constant of the first modes for this structure. The black dashed curve is the propagation constant of a plane wave, blue curves correspond to unwanted modes and the green curve with square marks is the desired mode. The propagation constant of a rectangular waveguide with same dimensions of the propagation channel of the GGW (i.e. $a_{RW} = 4.72$ mm, $b_{RW} = 2.775$ mm) is displayed for comparison in red. It can be seen that the band [28.1 GHz - 52.9 GHz] represents the stopband of the periodic structure, so that in such frequency range only the desired mode is propagating in the GGW.

In previous works, [13], [14], [20], it has been assumed that the equivalent of a GGW is a rectangular waveguide having the same propagation channel dimensions (i.e. $a_{RW} = a_{GGW}$, $b_{RW} = h_{a,GGW} + h_{p,GGW}$). However, when comparing the curves of the GGW with those of the rectangular waveguide (see Fig. 3) it can be seen that in the upper half of the stopband both curves are similar, but that this is not true near cutoff.

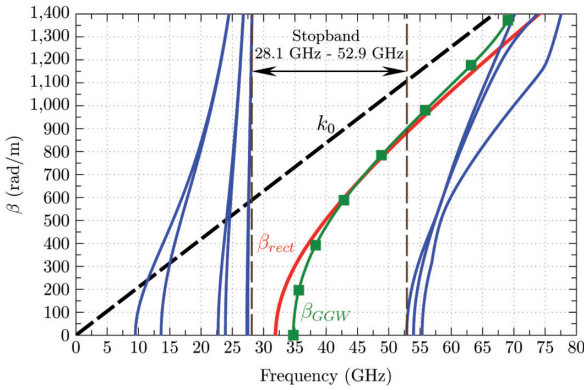
In fact, both waveguides present a different cutoff frequency, and even for frequencies where they are similar, a greater dispersive behavior is observed for the GGW structure.

To further characterize the propagation properties of GGW, the width of the propagation channel a is parameterized. To cover the possible cases of having cutoff

¹ For simplicity, in the rest of the text, the term VP will be omitted.



■ **Figure 2.** GGW cross-section and E-field distribution of its fundamental mode.

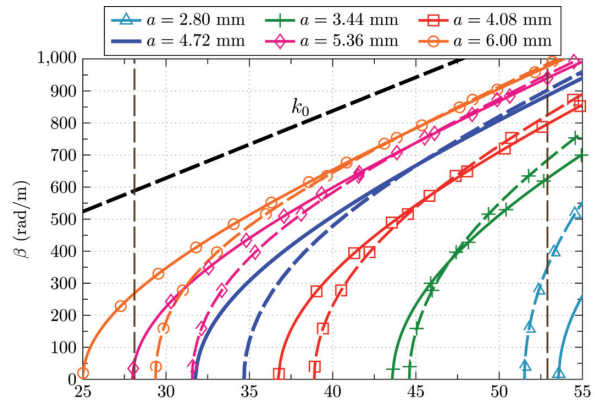


■ **Figure 3.** GGW dispersion diagram. Three lateral rows of pins are used.

going from near the minimum frequency of the stopband to the maximum frequency of the stopband, six values of a equally distributed between $a = 2.8 \text{ mm}$ and $a = 6 \text{ mm}$ are considered. The standard waveguide configuration is represented by the curve $a = 4.72 \text{ mm}$ [13].

The results of this parameterization are shown in Fig. 4. Here, in most cases, the GGW presents a higher cutoff frequency than its rectangular waveguide counterpart, especially as a increases. This means that GGW is effectively smaller in terms of propagating aperture than the equivalent rectangular waveguide assumed for each case (same physical aperture). The contrary could be expected since in GGW the fields are not strictly transmitted in the channel, but spread evanescently through the lateral pin regions. As a decreases, this difference becomes smaller and, if a is small enough ($a = 2.8 \text{ mm}$) the GGW has lower cutoff frequency than the rectangular waveguide, and becomes effectively larger than the equivalent rectangular waveguide.

In general, simulation reveals GGW to exhibit a greater dispersive behavior when compared with the equivalent rectangular waveguide. For the cases of larger a values, the GGW curve grows faster with frequency and reaches the rectangular waveguide curve, and, although β_{GGW} surpasses β_{rect} , both curves are quite similar from that point. For the cases of smaller a values, this difference is



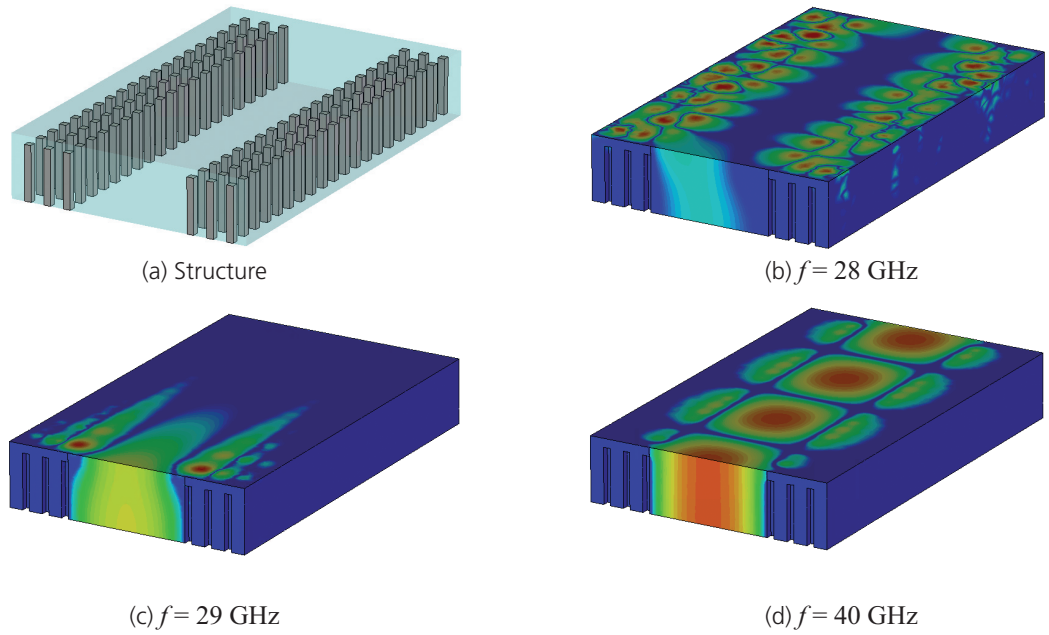
■ **Figure 4.** Propagation constant of the GGW and of the rectangular waveguide for different values of a . Solid lines correspond to the rectangular waveguide and dashed lines correspond to the GGW.

greater and both curves diverge having only a very narrow band of coincidence, or even no coincidence (e.g. at $a = 2.8 \text{ mm}$ where a very dispersive curve is observed.)

From the above study, it can be concluded that the standard assumption of equivalence between rectangular waveguide and GGW is only valid in certain bandwidth, which are determined by specific range values of a .

B. Operation below cutoff

In a below cutoff rectangular waveguide the lateral conditions are electric walls, and evanescent energy is delivered along the axial direction only. In the GGW, the condition of forbidden propagation into the pins regions also permits exponential decay as a lateral condition [17]. Consider the following example; the electric field is simulated for the case of a GGW with $a = 4.72 \text{ mm}$, which implies a cutoff of $f_c = 34.68 \text{ GHz}$. Since the stopband of the GGW structure starts at $f = 28.1 \text{ GHz}$, three frequencies are analyzed, $f = 28 \text{ GHz}$ (outside the stopband, mode below cutoff), $f = 29 \text{ GHz}$ (inside the stopband, mode below cutoff), and $f = 40 \text{ GHz}$ (inside the stopband, mode under usual operation above cutoff). The results of this comparison are shown in Fig. 5. As can be seen, outside the stopband, the field spreads into the pin structure, whereas inside the stopband energy is delivered along the axial direction in a similar manner to the rectangular waveguide in both cases, below and above cutoff. It is observed that the field spreads more in the lateral directions when the mode is below cutoff. This can be seen in Fig. 6 where the E_y component is plotted as a function of x on a transversal plane $z = z_0$ for different heights. The frequencies considered are $f = 29 \text{ GHz}$ (far below cutoff), $f = 34 \text{ GHz}$ (near below cutoff), $f = 40 \text{ GHz}$ (above, but near, cutoff), and $f = 52 \text{ GHz}$ (far above cutoff). It is seen that the field is better confined in the propagation channel as frequency increases. Near to cutoff axial attenuation is lower suggesting that the lateral conditions are presenting a higher attenuation path. Above cutoff lower interaction with the GGW lateral walls occur. It is worth to mention that in most of the structure (from $y = 0$ to $y = h_p$) the field correspond approximately



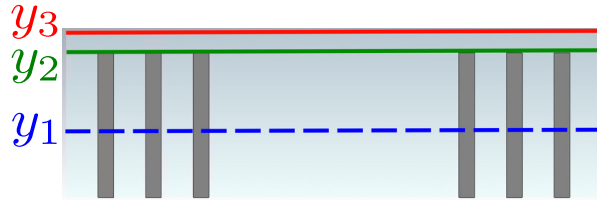
■ **Figure 5.** E_y field inside a GGW with $a = 4.72 \text{ mm}$ for different cases of propagation.

to the blue curve. These results suggest that GGW can operate below cutoff in an analogous manner to rectangular waveguide. However, the differences between both waveguides types are accentuated and local effects near or above the first row of pins must be taken into account.

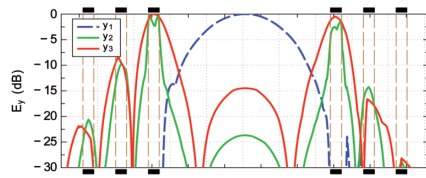
We now study the dispersion diagram of the structure under below cutoff operation. Above cutoff, it is sufficient to calculate the propagation constant of the GGW fundamental mode as indicated in [27], i.e. solving the

corresponding eigenvalue problem. Below cutoff we must simulate the whole structure, the one shown in Fig. 5(a), and then evaluate the following expression:

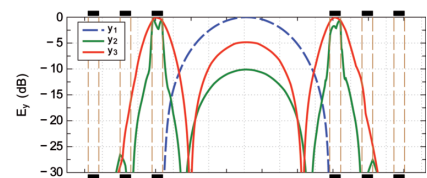
$$\alpha(\text{Np/m}) = \frac{\ln \left(\frac{E_y(z_1)}{E_y(z_2)} \right)}{z_1 - z_2} \quad (1)$$



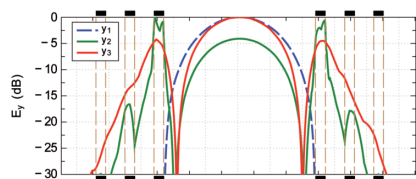
(a) Considered heights in y .



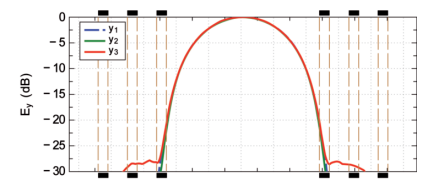
(b) $f = 29 \text{ GHz}$



(c) $f = 34 \text{ GHz}$

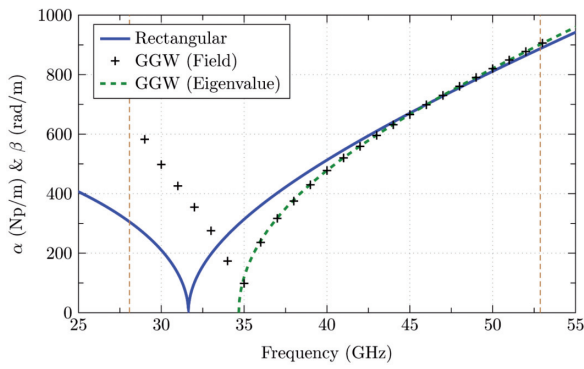


(d) $f = 40 \text{ GHz}$



(e) $f = 52 \text{ GHz}$

■ **Figure 6.** $E_y(x)$ GGW with $a = 4.72 \text{ mm}$ on a transversal plane at different heights y_i . Blue dashed line is $y_1 = h_p/2$, green line is $y_2 = h_p$, and red line is $y_3 = h_p + h_a$.



■ **Figure 7.** Propagation and attenuation constant for a rectangular waveguide and a GGW of $a = 4.72 \text{ mm}$.

here $z_1 > z_2$ and $E_y(z_i)$ is the amplitude of the E_y field component in the center of the waveguide ($x = a/2$) at the corresponding z -position.

The results of this study are shown in Fig. 7, which displays the attenuation and propagation constants of a rectangular waveguide (analytical) and a GGW (eigenvalue computation, and field computation of the full structure) for the case of $a = 4.72 \text{ mm}$.

Fig. 7 indicates that the difference between curves for both waveguide types continue increasing when the frequency goes below cutoff. It is seen that as the frequency decreases, the attenuation in the GGW grows faster than in the rectangular waveguide. Furthermore GGW exhibits growth as the stopband limit approaches instead of the expected slope decrease (as it happens with the rectangular waveguide). Similar results have been observed for other values of a , indicating that rectangular waveguide and GGW behave noticeably different below cutoff.

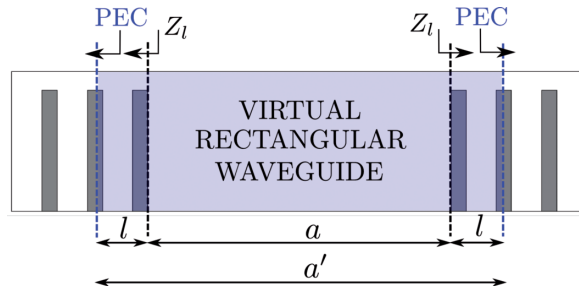
3. Proposed model

From the previous study, it is clear that the assumption of an equivalent behavior in a GGW and a rectangular waveguide with identical width a implies errors, unless f_c is near to the low stopband limit and the operation frequency is far enough from cutoff. Moreover, modelling this behavior is not possible by scaling the rectangular waveguide by a constant factor depending on the geometry (as it occurs with the Substrate Integrated Waveguide -SIW- [28]), since a frequency dependent behavior is observed. The shape of the obtained curves indicates that a mechanism is occurring within the structure, which involves the presence of a reactance due to the periodic lateral lattice.

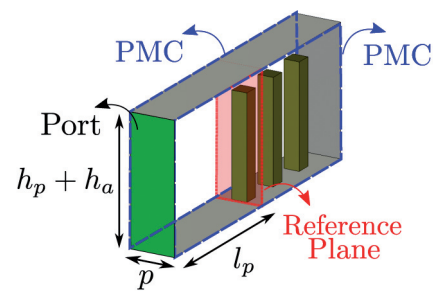
A. Proposed Method

Consider GGW, but now with regard to propagation in the lateral direction \hat{x} . The most interesting parameter in this configuration is the impedance Z_l that is seen when looking into the first row of pins (as shown in Fig. 8), where Z_l is the impedance of the waves incident on the side wall. The reference plane is placed on the first pin with the rest

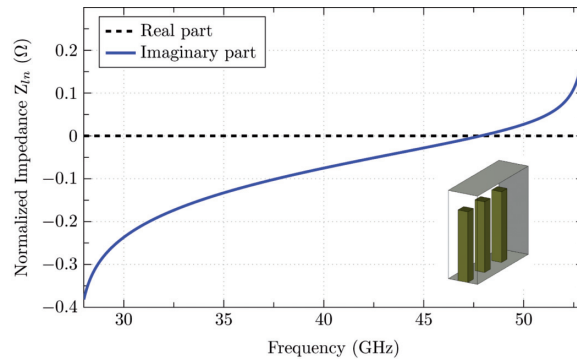
The GGW can operate below cutoff in an analogous manner to rectangular waveguide. However, the differences between both waveguides types are accentuated.



■ **Figure 8.** Schematic of the proposed method.



■ **Figure 9.** Schematic of the structure solved with CST to obtain Z_l .

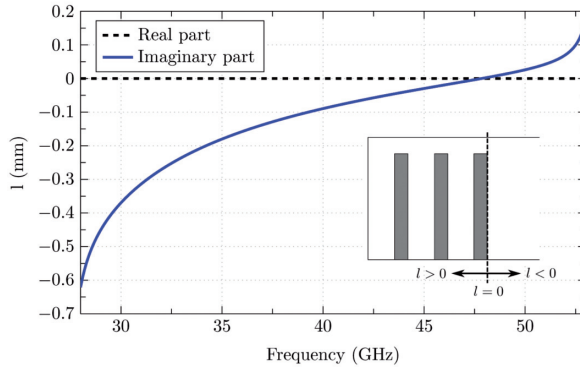


■ **Figure 10.** Lateral impedance viewed at the first pin row plane.

of the arrangement terminated with a perfect electric conductor (PEC), located at a distance of value $(p - w)$ with regard to the third pin. Periodicity is considered and only one period is analyzed, using PMC at the laterals (i.e., at $z = z_0$ and $z = z_0 + p$). Hence, referred to this port the normalized input impedance of the structure is

$$Z_{ln} = \frac{1 + S_{11}}{1 - S_{11}} \quad (2)$$

In order to obtain the required S_{11} parameter, the structure is simulated using CST, Fig. 9. In this figure it can be seen the PMC planes in blue, which provide periodicity by means of image theory, the unique port of the structure, in green, and the reference plane, in red. The



■ **Figure 11.** Distance l at which a PEC wall would produce the same impedance as the one of the periodic structure.

S_{11} parameter is easily obtained at the reference plane through de-embedding, and using (2), the normalized impedance Z_{ln} is calculated. For canonical shapes further reductions in computing time are possible using the methods proposed in [29]-[30]. With the model of Fig. 9 only a lateral row of three pins and a the vacuum volume of the auxiliar feeding parallel-plate $l_p \times p \times (h_p + h_a)$ are discretized and solved to determine its scattering parameters. Note that l_p can be made as small as desired and the discretizing cost of the auxiliar waveguide is negligible. The resulting normalized impedance obtained with this approach is shown in Fig. 10. We can see that the periodic structure presents a reactance that exhibits capacitive behavior at the beginning of the stopband, changing to inductive behavior at the end of the stopband and crossing zero at $f = 47,94$ GHz.

Let us now consider the normalized input impedance of transmission line of characteristic impedance Z_0 loaded with an impedance Z_L . If the transmission line is terminated with a short-circuit ($Z_L = 0$), the input impedance becomes

$$Z_{ln} = j \tan(\beta_p l) \quad (3)$$

hence

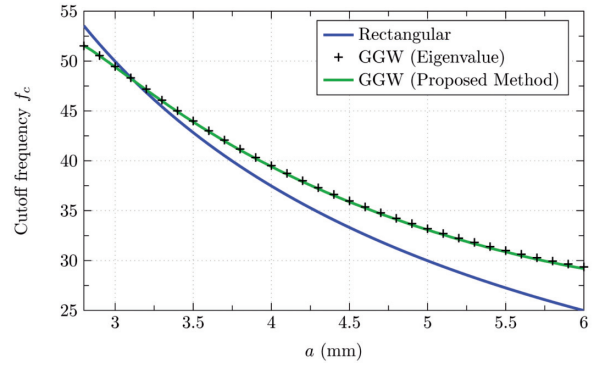
$$l = -\frac{1}{\beta_p} \tan^{-1}(jZ_{ln}) \quad (4)$$

where β_p is the propagation constant of the lateral parallel plate waveguide feeding the structure with three pins. Thus, the GGW is equivalent to a rectangular waveguide having lateral walls positioned at a distance which depends on Z_{ln} (and therefore on the frequency value). We have therefore a virtual rectangular waveguide with $a' = a + 2l$ (see Fig. 8).

Since for small arguments the function $\tan^{-1}(x)$ is almost linear and the β_p variation with frequency is small compared to the Z_L frequency variation, the behaviour of both Z_L and l is quite similar. Depending on the sign of l , the GGW will be equivalent to a smaller ($l < 0$) or a larger ($l > 0$) rectangular waveguide, as shown in the inset of Fig. 11.

B. Results

The cutoff frequency of the fundamental mode in a rectangular waveguide is:



■ **Figure 12.** Cutoff frequency f_c vs. waveguide width a .

$$f_c = \frac{c}{2a} \quad (5)$$

Since in the proposed model for the GGW the equivalent width a' depends on the frequency, the term f_c will also have this dependence. For a given frequency f_0 , one has $a'(f_0)$ and from (5), $f_c(f_0)$. In order to obtain the cutoff frequency for the GGW, a zero-finding routine is applied to $y(f) = f_c(f) - f$. Fig. 12 shows the cutoff frequency f_c as a function of a for both rectangular waveguide and GGW, comparing the solutions obtained with the eigenvalue method and the proposed model for the GGW. The CPU effort spent in the zero-finding routine is negligible.

The propagation or attenuation constant of the GGW can now be obtained through the standard rectangular waveguide formulas:

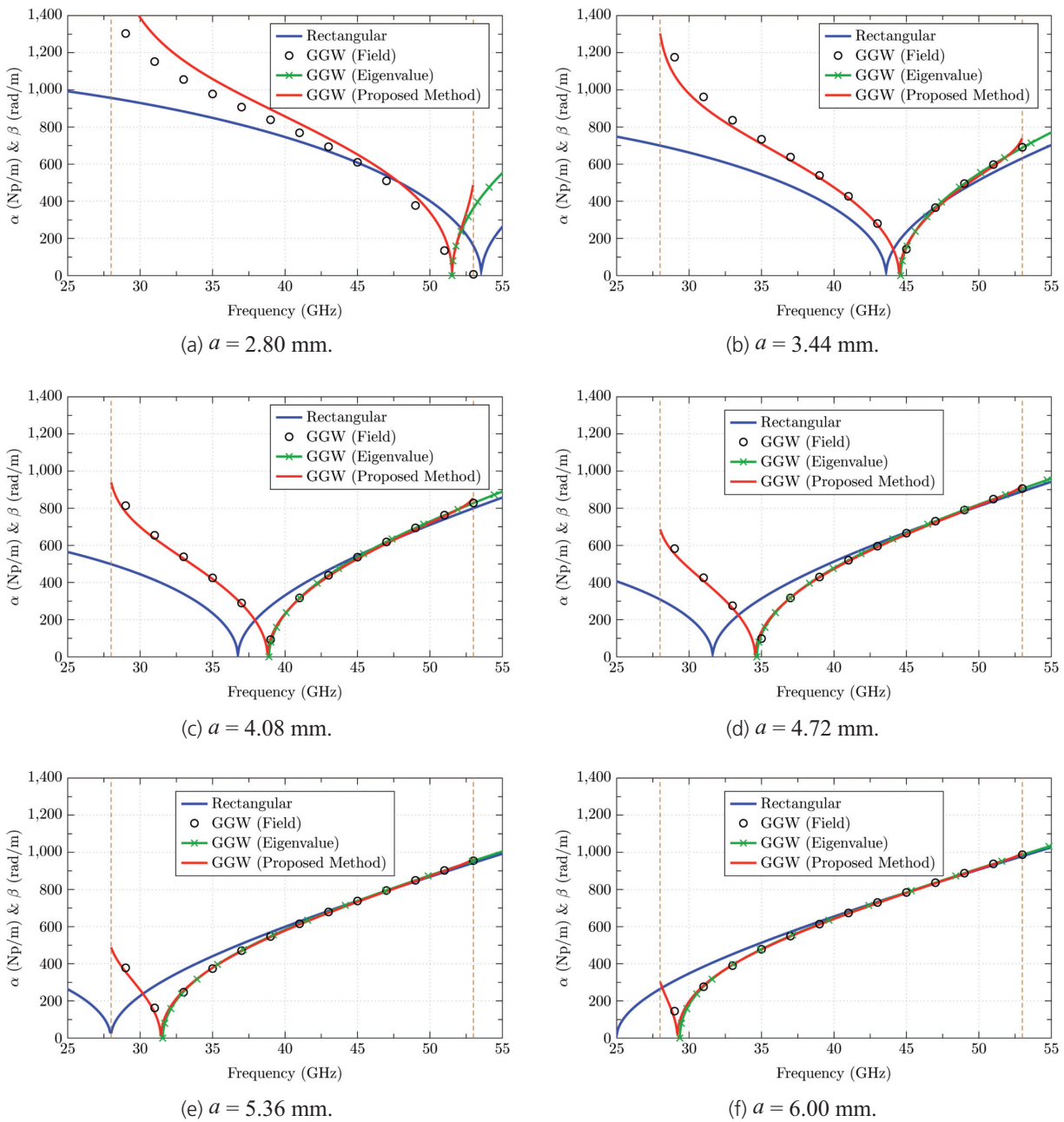
$$\beta = \sqrt{k^2 - \left(\frac{\pi}{a'}\right)^2} \quad f \geq f_c \quad (6)$$

$$\alpha = \sqrt{\left(\frac{\pi}{a'}\right)^2 - k^2} \quad f < f_c \quad (7)$$

In Fig. 13, it can be observed how the presented method shows good agreement with the other techniques based on intensive full-wave simulations (i.e. the one based on eigenvalues and the one using field evaluation).

Above cutoff, as a' grows with frequency (6) implies for GGW that β grows with the frequency faster than for the rectangular waveguide case. When the term k^2 is large compared with $(\pi/a')^2$ the variation of a' is less significant, and the propagation behavior is similar to that of a standard rectangular waveguide. This occurs for large values of a and high frequencies.

Below cutoff, as frequency is reduced, the term k^2 becomes small compared with $(\pi/a')^2$. Thus, with regard to (7), α exhibits growth with the decrease of a' with the frequency. This effect explains why the α curve of the GGW does not exhibit a reduction of its slope, as occurs with the rectangular waveguide when the frequency decreases. Therefore, below cutoff, the assumption of the rectangular waveguide as an equivalent GGW with



■ **Figure 13.** Propagation and attenuation constants of the rectangular waveguide and the GGW, comparing several calculations methods for the GGW case.

the same propagation channel dimensions implies a considerable error. Finally, it is worth to note that, due to the Foster Reactance Theorem [31], translated though (4), GGW should exhibit greater or equal dispersion than the equivalent rectangular waveguide.

To end this section a computation efficiency evaluation is carried out. The used computing machine incorporates an Intel® Xenon® CPU E3-1245 @ 3.40 GHz and 16 GB of RAM memory. Results shown in the table 1 correspond to the computation time given by CST® for each case.

The efficiency of the proposed method with regard to the other cases is clear. The simulation of the whole structure results in a heavy task because of the size, and

TABLE 1
COMPARISON OF CPU TIMES

	Computation time	Recalculation for different α
Field (full structure)	1380 s	YES
Eigenvalue (only β)	4230 s	YES
Proposed Method	24 s	NO

the solution of an eigenvalue problem is cumbersome, by nature [32]. In order to recover properly the requested data, several phase shifts and additional modes should be computed with the commercial software. Moreover,

The proposed model has a significantly reduced computational effort, thus being suitable for fast parametric analysis of GGWs and their efficient design through optimization algorithms.

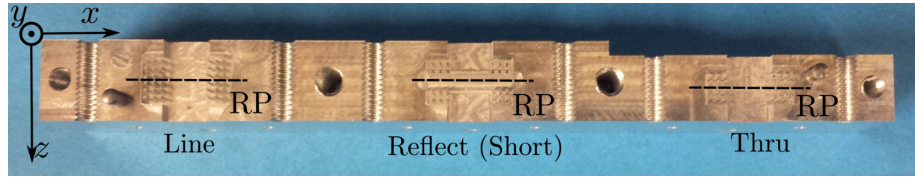
there is not possibility of solving the structure below cutoff with an eigenvalue simulation. In addition, a thoughtful post-processing is required, specially in the calculations involving the field at different frequencies (this additional effort has not been included in the comparison table).

Finally, a useful feature of this method is that, since the lateral impedance is independent of a , the same calculated values can be applied for different waveguide widths. This means that, for instance, that the cost of ob-

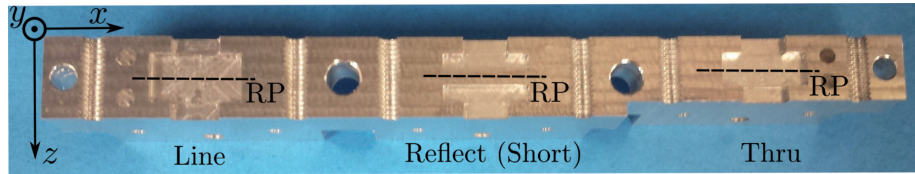
taining the data of all the graphs of the Fig. 13 is the same one requested for a graph if the proposed method is used. Contrarily, calculations corresponding to the field or the eigenvalue problem must be completely repeated for each case (value of a). Thus, due to its speed and additional physical insight, the proposed method appears to be an interesting tool for parametric analysis and optimized design of the GGW.

4. Experimental results

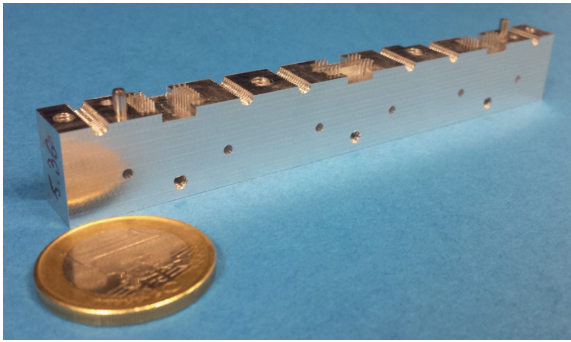
In order to validate the presented results, two TRL [33] calibration kits corresponding to the GGW widths $a = 4.08 \text{ mm}$ and $a = 5.36 \text{ mm}$ have been manufactured through an in-



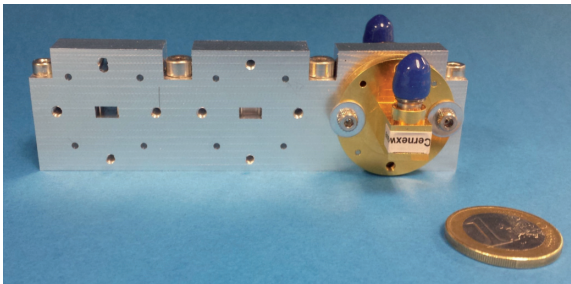
■ Figure 14. TRL calibration kit. Bottom piece containing the pins.



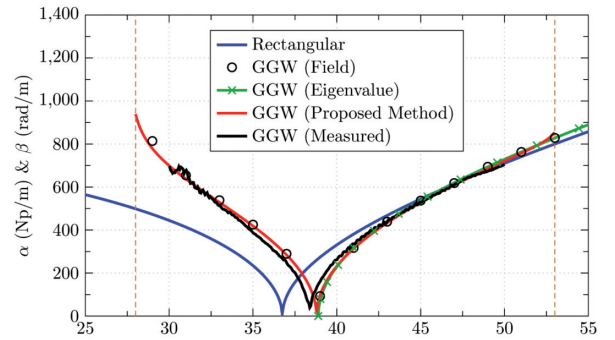
■ Figure 15. TRL calibration kit. Top piece.



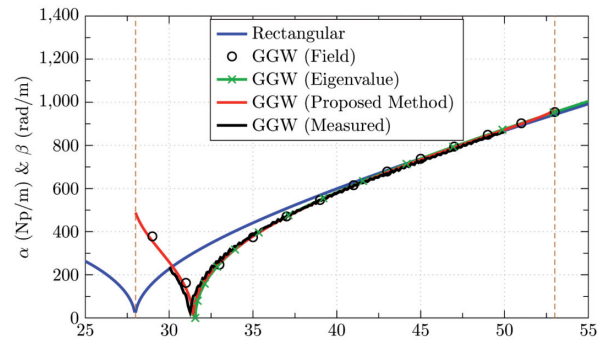
■ Figure 16. TRL calibration kit. Perspective view.



■ Figure 17. TRL calibration kit. Complete piece and WR-22 rectangular to coaxial transitions.



■ Figure 18. TRL Comparison between simulated and measured results, $a = 4.08 \text{ mm}$.



■ Figure 19. Comparison between simulated and measured results, $a = 5.36 \text{ mm}$.

house process using a DATRON® M25 milling system. Figs. 14 and 15 show the top and bottom piece, respectively, for one of the fabricated calibration kits. A perspective view of the bottom piece, where the metal pins can be clearly appreciated, is included in Fig. 16. Finally, the mounted calibration kit, including the transition from WR 22 to 2.4 mm coaxial is shown in Fig. 17. The use of the two different considered widths allows to further check that the presented method is properly obtaining the propagation constant in both cases, both below and above cutoff.

The corresponding measurements have been performed using a Keysight PNA N5227A Network Analyzer. Note that the TLR calibration algorithm allows to recover the complex propagation constant $\gamma = \alpha + j\beta$ of each waveguide. Thus, the TLR calibration kits let us to recover the propagation constant (or attenuation constant if the waveguide is below cutoff) for the cases $a = 4.08 \text{ mm}$ and $a = 5.36 \text{ mm}$. Comparisons between measured data and previous results (obtained with different methods) are shown in Fig. 18 and 19 for each case (a value). A good agreement is observed between the results obtained with the proposed method and the experimental curve. The slight frequency shift between both curves is justified by the precision of the in-house process, which is estimated to be about $\pm 10 \text{ }\mu\text{m}$ in the horizontal plane and $\pm 30 \text{ }\mu\text{m}$ in the vertical plane. The study performed in this section confirms that the novel proposed method provides a very accurate modelling of GGWs.

5. Conclusions

This paper has shown that the direct equivalent correspondence normally assumed between the GGW and rectangular waveguide, which is normally used in practice, is a rough approximation providing accurate results only for some specific cases. Also, for the first time, the behaviour of GGW below cutoff has been studied. This study has shown that the GGW and the rectangular waveguide behave in a very different way in terms of their dispersion characteristics. A simple method for the accurate analysis of GGW dispersion characteristics, based on equivalent short-circuited transmission lines, has been presented, and it has been shown to have very good prediction capability for all frequencies (below and above cutoff). The proposed model has a significantly reduced computational effort, thus being suitable for fast parametric analysis of GGWs and their efficient design through optimization algorithms. Using the proposed model it is deduced that the GGW is equivalent to a virtual rectangular waveguide whose width grows with the frequency. Two TLR calibration kits have been manufactured to obtain experimentally the dispersion curves of two GGWs. The good agreement observed between the measured and simulated results validates the proposed method.

Acknowledgments

This work was supported by the Spanish Ministerio de Economia y Competitividad under projects TEC2013-47360-C3-3-P and TEC2013-47037-C5-1-R, and by the Spanish Ministerio de Educacion under FPU research fellowship program AP2010-4227.

References

- [1] D. Lockie and D. Peck, "High-data-rate millimeter-wave radios," *IEEE Microwave Magazine*, vol. 10, no. 5, pp. 75–83, 2009.
- [2] J. Wells, "Faster than fiber: The future of multi-G/s wireless," *Microwave Magazine, IEEE*, vol. 10, no. 3, pp. 104–112, 2009.
- [3] T. S. Rappaport, S. Sun, R. Mayzus, H. Zhao, Y. Azar, K. Wang, G. N. Wong, J. K. Schulz, M. Samimi, and F. Gutierrez, "Millimeter wave mobile communications for 5G cellular: It will work!" *Access, IEEE*, vol. 1, pp. 335–349, 2013.
- [4] J. Hasch, E. Topak, R. Schnabel, T. Zwick, R. Weigel, and C. Wald-schmidt, "Millimeter-wave technology for automotive radar sensors in the 77 GHz frequency band," *IEEE Transactions on Microwave Theory and Techniques*, vol. 60, no. 3, pp. 845–860, 2012.
- [5] C. Yeh and F. Shimabukuro, *The essence of dielectric waveguides*. Springer Verlag, 2008.
- [6] M. N. Afsar, "Dielectric measurements of millimeter-wave materials," *IEEE Transactions on Microwave Theory and Techniques*, vol. 32, no. 12, pp. 1598–1609, 1984.
- [7] H. Shigesawa, M. Tsuji, and A. A. Oliner, "Simultaneous propagation of bound and leaky dominant modes on printed-circuit lines: A new general effect," *IEEE Transactions on Microwave Theory and Techniques*, vol. 43, no. 12, pp. 3007–3019, 1995.
- [8] F. Mesa, A. Oliner, D. Jackson, and M. J. Freire, "The influence of a top cover on the leakage from microstrip line," *IEEE Transactions on Microwave Theory and Techniques*, vol. 48, no. 12, pp. 2240–2248, 2000.
- [9] P.-S. Kildal, "Three metamaterial-based gap waveguides between parallel metal plates for mm/submm waves," in *3rd European Conference on Antennas and Propagation (EuCAP)*, 2009, pp. 28–32.
- [10] A. Valero-Nogueira, M. Baquero, J. I. Herranz, J. Domenech, E. Alfonso, and A. Vila, "Gap waveguides using a suspended strip on a bed of nails," *IEEE Antennas and Wireless Propagation Letters*, vol. 10, pp. 1006–1009, 2011.
- [11] E. Rajo-Iglesias and P.-S. Kildal, "Groove gap waveguide: A rectangular waveguide between contactless metal plates enabled by parallel-plate cut-off," in *4th European Conference on Antennas and Propagation (EuCAP)*. IEEE, 2010, pp. 1–4.
- [12] E. Alfonso, A. Zaman, and P. Kildal, "Ka-band gap waveguide coupled-resonator filter for radio link diplexer application," *IEEE Transactions on Components, Packaging and Manufacturing Technology*, vol. 3, no. 5, pp. 870–879, 2013.
- [13] A. del Olmo-Olmeda, M. Baquero-Escudero, V. E. Boria-Esbert, A. Valero-Nogueira, and A. Berenguer, "A novel band-pass filter topology for millimeter-wave applications based on the groove gap waveguide," in *International Microwave Symposium*. IEEE, 2013, pp. 1–4.
- [14] A. U. Zaman, P.-S. Kildal, and A. A. Kishk, "Narrow-band microwave filter using high-Q groove gap waveguide resonators with manufacturing flexibility and no sidewalls," *IEEE Transactions on Components, Packaging and Manufacturing Technology*, vol. 2, no. 11, pp. 1882–1889, 2012.

- [15] S. Martinez Giner, A. Valero-Nogueira, J. Herranz Herruzo, and M. Baquero Escudero, "Excitation of untilted narrow-wall slot in groove gap waveguide by using a parasitic dipole," in *7th European Conference on Antennas and Propagation (EuCAP)*, 2013, pp. 3082–3085.
- [16] E. Rajo-Iglesias and P.-S. Kildal, "Numerical studies of bandwidth of parallel-plate cut-off realised by a bed of nails, corrugations and mushroom-type electromagnetic bandgap for use in gap waveguides," *IET microwaves, antennas & propagation*, vol. 5, no. 3, pp. 282–289, 2011.
- [17] A. Polemi and S. Maci, "Closed form expressions for the modal dispersion equations and for the characteristic impedance of a metamaterial-based gap waveguide," *IET Microwaves, Antennas & Propagation*, vol. 4, no. 8, pp. 1073–1080, 2010.
- [18] M. Bosiljevac, A. Polemi, S. Maci, and Z. Sipus, "Analytic approach to the analysis of ridge and groove gap waveguides-comparison of two methods," in *5th European Conference on Antennas and Propagation (EuCAP)*. IEEE, 2011, pp. 1886–1889.
- [19] M. Bosiljevac, Z. Sipus, and P.-S. Kildal, "Construction of green's functions of parallel plates with periodic texture with application to gap waveguides - a plane-wave spectral-domain approach," *IET Microwaves, Antennas Propagation*, vol. 4, no. 11, pp. 1799–1810, 2010.
- [20] H. Raza, J. Yang, P.-S. Kildal, and E. Alfonso, "Resemblance between gap waveguides and hollow waveguides," *IET Microwaves, Antennas Propagation*, pp. 1–7, 2013.
- [21] G. F. Craven and C. Mok, "The design of evanescent mode waveguide bandpass filters for a prescribed insertion loss characteristic," *IEEE Transactions on Microwave Theory and Techniques*, vol. 19, no. 3, pp. 295–308, 1971.
- [22] G. F. Craven and R. F. Skedd, *Evanescent mode microwave components*, 1987, vol. 1.
- [23] P. Ludlow and V. Fusco, "Reconfigurable small-aperture evanescent waveguide antenna," *IEEE Transactions on Antennas and Propagation*, vol. 59, no. 12, pp. 4815–4819, 2011.
- [24] P. Ludlow, V. Fusco, G. Goussetis, and D. E. Zelenchuk, "Applying band-pass filter techniques to the design of small-aperture evanescent-mode waveguide antennas," *IEEE Transactions on Antennas and Propagation*, vol. 61, no. 1, pp. 134–142, 2013.
- [25] E. Pucci, A. Zaman, E. Rajo-Iglesias, P.-S. Kildal, and A. Kishk, "Study of q-factors of ridge and groove gap waveguide resonators," *IET Microwaves, Antennas Propagation*, vol. 7, no. 11, pp. 900–908, 2013.
- [26] C. C. S. Technology, "CST studio suite," 2013, Suite 2013, Germany.
- [27] P.-S. Kildal, A. Zaman, E. Rajo-Iglesias, E. Alfonso, and A. Valero-Nogueira, "Design and experimental verification of ridge gap waveguide in bed of nails for parallel-plate mode suppression," *IET Microwaves, Antennas Propagation*, vol. 5, no. 3, pp. 262–270, 2011.
- [28] W. Che, K. Deng, D. Wang, and Y. Chow, "Analytical equivalence between substrate-integrated waveguide and rectangular waveguide," *IET microwaves, antennas & propagation*, vol. 2, no. 1, pp. 35–41, 2008.
- [29] G. Conciauro, M. Bressan, and C. Zuffada, "Waveguide modes via an integral equation leading to a linear matrix eigenvalue problem," *IEEE Transactions on Microwave Theory and Techniques*, vol. 32, no. 11, pp. 1495–1504, 1984.
- [30] H. Auda and R. F. Harrington, "Inductive posts and diaphragms of arbitrary shape and number in a rectangular waveguide," *IEEE Transactions on Microwave Theory and Techniques*, vol. 32, no. 6, pp. 606–613, 1984.
- [31] R. M. Foster, "A reactance theorem," *Bell System Technical Journal*, vol. 3, no. 2, pp. 259–267, 1924.
- [32] L. N. Trefethen and D. Bau III, *Numerical linear algebra*. Siam, 1997, vol. 50.
- [33] G. F. Engen and C. A. Hoer, "Thru-reflect-line: An improved technique for calibrating the dual six-port automatic network analyzer," *IEEE Transactions on Microwave Theory and Techniques*, vol. 27, no. 12, pp. 987–993, 1979.

Biographies



Antonio Berenguer was born in Onil (Alicante), Spain in May 1st, 1987. He received the Telecommunication Engineering degree in 2010 and M.S. degree in electrical engineering in 2011, both with honours from the Universitat Politècnica de València (UPV). He has been awarded with the Second Prize for the Best Final Degree Project in Security and Defense of the National College of Electrical Engineers (COIT) in 2010, and with the Best Academic Record of the Master's Degree in Communication Technologies, Systems and Networks (UPV) in 2011. In 2014, his paper was finalist of the Young Engineer Prize at the European Microwave Conference.

He has been with the Institute of Telecommunications and Multimedia Applications (ITEAM) of the UPV since 2010. He is currently working towards the Ph.D. degree in electrical engineering with a FPU fellowship from the Spanish government, and towards the Bachelor Degree in Mathematics in the National Distance Education University (UNED). Since 2013, he has also held several lecturing positions at the UPV. His main research interests include terahertz technology, modal analysis of surface waveguides, numerical methods, optimization algorithms, and analysis and design of passive components on Gap Waveguide technology.



Vincent Fusco holds a personal chair in High Frequency Electronic Engineering at the Queens University of Belfast. His research interests include active antenna and front-end MMIC techniques. He is head of the High Frequency Laboratories at QUB where he is also director of the International Centre for System on Chip for Advanced Microwaveless.

Professor Fusco has published over 450 scientific papers in major journals and in referred international conferences. He has authored two text books, holds patents related to self-tracking antennas and has contributed many invited papers and book chapters. He serves on the technical

programme committee for various international conferences including the European Microwave Conference.

He is a Fellow of both the Institution of Engineering and Technology and the Institute of Electrical and Electronic Engineers. In addition he is a Fellow of the Royal Academy of Engineers and a member of the Royal Irish Academy.



Dmitry E. Zelenchuk (S'02, M'05, SM'14) received his PhD in Radiophysics from Rostov State University (Russia) in 2004.

From 2003 till 2005 he was a Lecturer at the Dept. of Applied Electrodynamics and Computer Modelling, Rostov State University, Russia. Currently he is with Queen's University Belfast, UK. His research

interests include electromagnetic field theory, material characterization; mm-wave circuits, antennas and advanced packaging; propagation in complex environments; and various physical phenomena of plasmonic and nanostructures. He has published more than 80 journal and conference papers and a book chapter and been a session chair at scientific conferences.

In 2001 Dr. Zelenchuk was awarded the medal of Ministry of Education of the Russian Federation "For the Best Scientific Student Paper".



Daniel Sánchez-Escuderos (M'05) was born in Vila-real, Spain, on October 20, 1980. He received the degree in telecommunications engineering and the Ph.D. degree from the Universitat Politècnica de València (UPV), Valencia, Spain, in 2004 and 2009, respectively. He became a Member of the IEEE in 2005.

Since 2005, he is with the Institute of Telecommunications and Multimedia Application of the Universitat Politècnica de València. In 2005, he was granted with a FPI national scholarship to course the doctorate studies, and in 2009 he was contracted as a post-doc in the framework of a national research project in THz technology. Since 2014 he is collaborating in a European project financed by the European Space Agency. His main research interests include antenna measurements, FSS structures, millimetre and submillimetre-wave technology and microwave filters.



Mariano Baquero-Escudero (S'87-M'90) was born in Murcia, Spain, on January 11, 1962. He received the degree in telecommunications engineering from the Polytechnic University of Catalonia (UPC), Barcelona, Spain, in 1986 and the Ph.D. degree from the Polytechnic University of Valencia (UPV), Valencia, Spain, in 1994. He became a

Member (M) of IEEE in 1987.

He was with the Antennas, Microwave and Radar Group, UPC, from 1986 to 1988, where he worked on the development of a cylindrical near-field facility to measure a 3-D radar antenna in CESELSA. Since 1989, he has been with the UPV where he became a Full Professor in 2003. During 1995, he held a postdoctoral grant at the Joint Research Centre, European Commission, Ispra, Italy, where he developed high-resolution algorithms for radar applications. From April 1996 to February 1998, he was a Vice-Dean of the Telecommunications Engineering School of Valencia. He is currently with the Communications Department and into the Institute of Telecommunications and Multimedia Application of the Polytechnic University of Valencia. His main research interests include microwave circuit and antenna analysis, design and measurement.



Vicente E. Boria (S'91-A'99-SM'02) was born in Valencia, Spain, on May 18, 1970. He received his "Ingeniero de Telecomunicación" degree (with first-class honors) and the "Doctor Ingeniero de Telecomunicación" degree from the Universidad Politécnica de Valencia, Valencia, Spain, in 1993 and 1997, respectively.

In 1993 he joined the "Departamento de Comunicaciones", Universidad Politécnica de Valencia, where he has been Full Professor since 2003. In 1995 and 1996, he was holding a Spanish Trainee position with the European Space Research and Technology Centre, European Space Agency (ESTEC-ESA), Noordwijk, The Netherlands, where he was involved in the area of EM analysis and design of passive waveguide devices. He has authored or co-authored 7 chapters in technical textbooks, 75 papers in refereed international technical journals, and over 150 papers in international conference proceedings. His current research interests are focused on the analysis and automated design of passive components, left-handed and periodic structures, as well as on the simulation and measurement of power effects in passive waveguide systems.

Dr. Boria has been a member of the IEEE Microwave Theory and Techniques Society (IEEE MTT-S) and the IEEE Antennas and Propagation Society (IEEE AP-S) since 1992. He is member of the Editorial Boards of the IEEE Transactions on Microwave Theory and Techniques, IEEE Microwave and Wireless Components Letters, Proceedings of the IET (Microwaves, Antennas and Propagation), IET Electronics Letters and Radio Science. Since 2013, he serves as Associate Editor of IEEE Microwave and Wireless Components Letters. He is also a member of the Technical Committees of the IEEE-MTT International Microwave Symposium and of the European Microwave Conference.



Alejandro Valero-Nogueira was born in Madrid, Spain on July 19, 1965. He received the M.S. degree in electrical engineering from Universidad Politécnica de Madrid, Madrid, Spain in 1991 and the Ph.D. degree in electrical engineering from Universidad Politécnica de Valencia, Valencia, Spain in 1997. In 1992 he joined

the Departamento de Comunicaciones, Universidad Politécnica de Valencia, where he is currently an Associate Professor. During 1999 he was on leave at the Electro-Science Laboratory, The Ohio State University, Columbus, where he was involved in fast solution methods in electromagnetics and conformal antenna arrays. His current research interests include computational electromagnetics, gap waveguides, waveguide slot arrays, millimetre-wave technology and automated antenna design procedures.



Miguel Ferrando-Bataller was born in Alcoy, Spain, in 1954. He received the M.S. and Ph.D. degrees in telecommunication engineering from the Universitat Politècnica de Catalunya, Barcelona, Spain in 1977 and 1982, respectively.

From 1977 to 1982, he was a Teaching Assistant in the Antennas, Microwave and Radar Group, Universitat Politècnica de Catalunya and in 1982, became an Associate Professor.

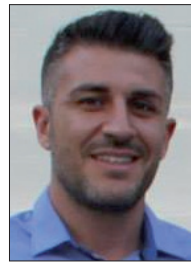
In 1990, he joined the Universidad Politécnica de Valencia, Spain, as Professor. He was Director of the Telecommunication Engineering School (1991-96), Vice-Chancellor (1996-99, 2005-2009) and Director of Long-life learning Office (2009-2013). Currently he is teaching antennas, advanced electromagnetics and satellite communications. The research interest includes numerical methods, UWB antennas, mm-wave antennas and e-learning activities.



Miguel Ferrando was born in Alcoy, Spain in 1985. He obtained his M.Sc. in Telecommunication Engineering by Universitat Politècnica de València (UPV) in 2012. In 2010 he received a Erasmus grant for Ghent University in Belgium where he was involved in several projects in the Department of Information Technology.

In November 2012 he joined as a researcher in the Complex Radiation Systems team of the Institute of Electronics and Telecommunications of Rennes (IETR) in France where he worked on Reflectarray Antennas for Satellite Applications in collaboration with Thales Alenia Space.

Since September 2013 he works in the Electromagnetic Radiation Group of the Institute of Telecommunications and Multimedia Applications of the Universitat Politècnica de València (Spain). Currently, he is a PhD grant holder from the Spanish Ministry of Economy and Competitiveness under the FPI program.



Tomás Bernabeu-Jiménez received the Licenciado degree in physics from the University of Valencia, and the master's degree in telecommunications from the Polytechnical University of Valencia, Valencia, Spain, in 2010 and 2013, respectively. He is currently pursuing the Ph.D. degree in Telecommunications with the Polytechnical University of Valencia. His current research interests include characteristic modes analysis on dielectric bodies.



Felipe Vico was born in Valencia, Spain, in 1981. He received the M.S degree in 2004 in Telecommunication engineering from the Polytechnic University of Valencia and the Ph.D. degree in 2009 in Telecommunications engineering also from UPV. He received the M.S in Mathematics in 2009 from Universidad Nacional de Educación a Distancia.

He received the best paper award in EUCAP 2006. During 2010 he stayed for several months as a guest researcher at the Courant Institute of Mathematical Sciences, in New York City, USA. He is now assistant Professor in Universidad Politécnica de Valencia. His research interests are Numerical methods for CEM, high frequency methods and integral equation methods.